

Distributionally Adversarial Attack

Tianhang Zheng, Changyou Chen, Kui Ren

Department of Computer Science and Engineering,
State University of New York at Buffalo

Abstract

Recent work on adversarial attack has shown that Projected Gradient Descent (PGD) Adversary is a universal first-order adversary, and the classifier adversarially trained by PGD is robust against a wide range of first-order attacks. However, it is worth noting that the objective of an attacking/defense model relies on a data distribution, typically in the form of risk maximization/minimization: $\max/\min \mathbb{E}_{p(\mathbf{x})} \mathcal{L}(\mathbf{x})$, with $p(\mathbf{x})$ the data distribution and $\mathcal{L}(\cdot)$ a loss function. While PGD generates attack samples independently for each data point, the procedure does not necessarily lead to good generalization in terms of risk maximization. In the paper, we achieve the goal by proposing distributionally adversarial attack (DAA), a framework to solve an optimal *adversarial data distribution*, a perturbed distribution that is close to the original data distribution but increases the generalization risk maximally. Algorithmically, DAA performs optimization on the space of probability measures, which introduces direct dependency between all data points when generating adversarial samples. DAA is evaluated by attacking state-of-the-art defense models, including the adversarially trained models provided by MadryLab. Notably, DAA outperforms all the attack algorithms listed in MadryLab’s white-box leaderboard, reducing the accuracy of their secret MNIST model to 88.79% (with l_∞ perturbations of $\epsilon = 0.3$) and the accuracy of their secret CIFAR model to 44.73% (with l_∞ perturbations of $\epsilon = 8.0$). Code for the experiments is released on <https://github.com/tianzheng4/Distributionally-Adversarial-Attack>

1 Introduction

Recent years have witnessed wider-spread use of deep neural networks (DNNs), achieving remarkable performance in different machine-learning tasks, such as object detection and recognition (Krizhevsky, Sutskever, and Hinton 2012), strategy optimization (Silver et al. 2016), and language processing (Cho et al. 2014). On the other hand, DNNs also have been proved to be vulnerable to adversarial samples – data that is indistinguishable from natural samples by human but endow additional maliciously-embedded perturbations. Those maliciously perturbed samples can cause DNNs to make predictions different from the ground truth with high confidence. Various first-order algorithms have been proposed to generate adversarial samples, such as Fast Gradient Sign Method (FGSM) (Goodfellow, Shlens, and Szegedy

2014), Projected Gradient Descent (PGD) (Kurakin, Goodfellow, and Bengio 2016b), and Carlini & Wagner Attacks (CW) (Carlini and Wagner 2017).

Among all those first-order attacks, Madry et al. suggest that PGD is a universal attack algorithm, and the classifier adversarially trained by PGD is robust against a wide range of first-order attacks (Madry et al. 2017). Carlini et al. strengthen the hypothesis by demonstrating that PGD-adversarial training provably succeeds at increasing the distortion required to construct adversarial examples by a factor of 4.2 (Carlini et al. 2017). Moreover, among all the 8 defenses submitted to ICLR2018, PGD-adversarial training is the only defense that has far not been successfully attacked (Athalye, Carlini, and Wagner 2018).

Despite the success of PGD, one notable limitation is that the adversarial samples are not globally optimal, in the sense that adversarial samples are generated independently based on each data point. From a machine-learning perspective, this lacks a statistical interpretation in terms of risk maximization, *i.e.*, PGD is not a training procedure, thus the underlying optimization problem is not mathematically clear. In this paper, we provide a distribution-optimization view of PGD, and propose distributionally adversarial attacking (DAA), a new concept of adversarial attack that is performed on the space of probability measures (unknown data distributions). In DAA, the problem is formulated as optimizing an adversarial data distribution (from which adversarial samples are drawn from) such that the *generalization risk* increases maximumly. This generalizes PGD by lifting the optimization onto space of probability distribution, and can be interpreted as Wasserstein gradient flows (WGFs), a framework of distribution optimization which always decreases an “energy functional” over time. The energy functional reflexes the data manifold in our case, and it is designed in correspondence to the original objective of a DNN. When using testing data to approximate the unknown data manifold, DAA leads to a variant of the standard PGD, where all adversarial samples are explicitly dependent.

DAA is extensively evaluated on four datasets, including MNIST, FMNIST, CIFAR10, and Imagenet, by attacking their state-of-the-art defense models. We show that a single run of DAA with 0.3/1.0 l_∞ perturbations can reduce the accuracy of MadryLab’s MNIST model (Madry et al. 2017) to approximately 90.5%, outperforming a single run of PGD

that reduces the accuracy to approximately 92.5%. Furthermore, a single run of DAA with 0.2/1.0 l_∞ perturbations reduces the accuracy of our adversarially trained FMNIST model to 67.6%, outperforming a single run of PGD that reduces the accuracy to 71.5%. Similarly, a single run of DAA reduces the accuracy of MadryLab’s CIFAR10 model to 44.98% (8/255 l_∞ perturbations) and the accuracy of the ensemble adversarial trained Imagenet model (Kurakin, Goodfellow, and Bengio 2016b) to 16.43% (only 2/255 l_∞ perturbations). For DAA with 50 random restarts, it reduces the accuracy of MadryLab’s public/secret MNIST model to 88.7%/88.79%; whereas DAA with 10 random restarts reduces the accuracy of MadryLab’s secret CIFAR10 model to 44.73%. Both settings outperform other attack algorithms listed in MadryLab’s white-box leaderboard.

2 Preliminaries

We introduce necessary background in this section, including Wasserstein gradient flows and adversarial attack/defense methods.

2.1 Wasserstein Gradient Flows

Wasserstein Metric Space Wasserstein metric is a distance metric defined between probability measures (distributions) on the Wasserstein metric space. Formally, let $P_2(\Omega)$ denote the collection of all probability measures on $\Omega \subset \mathbb{R}^r$ with finite 2nd moment. The 2nd-order Wasserstein distance between two probability measures in $P_2(\Omega)$ is defined as:

$$W_2^2(\mu, \nu) \triangleq \inf_{\gamma} \left\{ \int_{\Omega \times \Omega} \|\mathbf{x} - \mathbf{x}'\|_2^2 d\gamma(\mathbf{x}, \mathbf{x}') : \gamma \in \Omega(\mu, \nu) \right\},$$

where $\Gamma(\mu, \nu)$ denotes the collection of all joint probability measures on $\Omega \times \Omega$ with two marginals equal to μ and ν . One way to understand the motivation of the above definition is to consider the optimal transport problem, where one wants to transform elements in the domain of μ to ν with minimum cost. The cost to transport \mathbf{x} in μ to \mathbf{x}' in ν is quantified by $\|\mathbf{x} - \mathbf{x}'\|_2^2$. If μ is absolutely continuous w.r.t. the Lebesgue measure, there exists a unique optimal transport plan, i.e., a mapping $T : \mathbb{R}^r \rightarrow \mathbb{R}^r$, to transform elements in μ to elements in ν . The Wasserstein distance can be equivalently reformulated as: $W_2^2(\mu, \nu) \triangleq \inf_T \left\{ \int_{\Omega} \|\mathbf{x} - T(\mathbf{x})\|_2^2 d\mu(\mathbf{x}) \right\}$.

Wasserstein Gradient Flows The 2nd-order Wasserstein metric endows $P_2(\Omega)$ with a Riemannian geometry. Let $\{\mu_t\}_{t \in [0,1]}$ be an absolutely continuous curve on this geometry, with distance between μ_t and μ_{t+h} measured by $W_2^2(\mu_t, \mu_{t+h})$. The change can be reflected by a vector field: $v_t(\mathbf{x}) \triangleq \lim_{h \rightarrow 0} \frac{T(\mathbf{x}) - \mathbf{x}}{h}$. This vector field is regarded as the velocity field of the elements \mathbf{x} . Based on the above setup, a gradient flow can be defined on $P_2(\Omega)$ in Lemma 1.

Lemma 1 *Let $\{\mu_t\}_{t \in [0,1]}$ be an absolutely continuous curve in $P_2(\Omega)$. Then for a.e. $t \in [0,1]$, the above vector field \mathbf{v}_t defines a gradient flow on $P_2(\Omega)$ as: $\partial_t \mu_t + \nabla \cdot (\mathbf{v}_t \mu_t) = 0$.*

Actually, the velocity field \mathbf{v} can be derived from an energy functional $E : P_2(\Omega) \rightarrow \mathbb{R}$. It can be shown that \mathbf{v}_t has

the form $\mathbf{v}_t = -\nabla \frac{\delta E}{\delta \mu_t}$ (Ambrosio, Gigli, and Savaré 2008), where $\frac{\delta E}{\delta \mu_t}$ is called the first variation of E at μ_t . Thus the gradient flow on $P_2(\Omega)$ can be rewritten as:

$$\partial_t \mu_t = -\nabla \cdot (\mathbf{v}_t \mu_t) = \nabla \cdot (\mu_t \nabla \frac{\delta E}{\delta \mu_t}) \quad (1)$$

2.2 Adversarial Sample

Definition and Notation In this paper, we only study adversarial samples on neural networks used for classification, with final layers as softmax activation functions. We represent such a network as a vector function $\{F_i(\mathbf{x})\}_i$. Given an input \mathbf{x} , the network predicts its label as $\tilde{y} = \arg_i \max F_i(\mathbf{x})$. A sample \mathbf{x}' is called an adversarial sample if $\arg_i \max F_i(\mathbf{x}') \neq y$, where y is the true label and \mathbf{x}' is close to the original \mathbf{x} under a certain distance metric.

Fast Gradient Sign Method (FGSM) Fast Gradient Sign Method (FGSM) is a single-step adversarial attack proposed by (Goodfellow, Shlens, and Szegedy 2014). FGSM performs a single step update on the original sample \mathbf{x} along the direction of the gradient of a loss function $\mathcal{L}(\mathbf{x}, y; \theta)$. The loss function is usually defined as the cross-entropy between the output of a network and the true label y . Formally, FGSM adversarial samples are generated as

$$\mathbf{x}' = \text{clip}_{[0,1]} \{ \mathbf{x} + \epsilon \cdot \text{sign}(\nabla_{\mathbf{x}} \mathcal{L}(\mathbf{x}, y; \theta)) \}, \quad (2)$$

where ϵ controls the maximum l_∞ perturbation of the adversarial samples, and the $\text{clip}_{[a,b]}(\mathbf{x})$ function forces \mathbf{x} to reside in the range of $[a, b]$.

Projected Gradient Descent (PGD) Projected Gradient Descent (PGD) is an iterative variant of FGSM. In each iteration, PGD follows the update rule:

$$\mathbf{x}'_{l+1} = \Pi_{\text{clip}} \{ \text{FGSM}(\mathbf{x}'_l) \}, \quad (3)$$

where $\text{FGSM}(\mathbf{x}'_l)$ represents an FGSM update of \mathbf{x}'_l as in (2), and the outer clip function Π_{clip} keeps \mathbf{x}'_{l+1} within a pre-defined perturbation range. PGD can also be interpreted as an iterative algorithm to solve the following problem:

$$\max_{\mathbf{x}' : \|\mathbf{x}' - \mathbf{x}\|_\infty < \alpha} \mathcal{L}(\mathbf{x}', y; \theta). \quad (4)$$

(Madry et al. 2017) observes that the local maxima of the cross-entropy loss found by PGD with 10^5 random starts are distinct, but all have similar loss values, for both normally and adversarially trained networks. Inspired by this concentration phenomena, they propose that PGD is a universal adversary among all the first-order adversaries, i.e., attacks only rely on first-order information.

Momentum-based Iterative Fast Gradient Sign Method (MI-FGSM) MI-FGSM is derived from the Iterative FGSM (Kurakin, Goodfellow, and Bengio 2016a), which integrates the momentum term into the iterative process to generate adversarial samples (Dong et al. 2018). Given

$g_0 = 0$ and $g_{l+1} = \mu \cdot g_l + \frac{\nabla_x \mathcal{L}(\mathbf{x}'_l, y; \theta)}{\|\nabla_x \mathcal{L}(\mathbf{x}'_l, y; \theta)\|_1}$, the iterative version of MI-FGSM can be expressed as:

$$\mathbf{x}'_{l+1} = \mathbf{x}'_l + \epsilon \cdot \text{sign}(g_{l+1}). \quad (5)$$

Based on MI-FGSM, we further derive its PGD variant, Momentum PGD, whose iterative version follows

$$\mathbf{x}'_{l+1} = \mathbf{x}'_l + \Pi_{clip}\{\epsilon \cdot \text{sign}(g_{l+1})\}. \quad (6)$$

Remark 2 *Momentum PGD is a stronger attack than MI-FGSM, since it can proceed for more steps with an appropriate step size ϵ (ϵ can not be too small, otherwise the adversarial samples are very likely to get trapped in bad local maxima). The clip function Π_{clip} ensures the adversarial samples to have the predefined perturbation size after the extra iterations.*

2.3 Adversarial Training

Definition and Notation Adversarial training is a defense method against adversarial samples first proposed by Szegedy et al.. The approach attempts to improve the robustness of a network by training it together with adversarial samples. Formally, adversarial training solves the following min-max problem:

$$\min_{\theta} \max_{\mathbf{x}': D(\mathbf{x}, \mathbf{x}') < \alpha} \mathcal{L}(\mathbf{x}', y; \theta), \quad (7)$$

where $D(\mathbf{x}, \mathbf{x}')$ represents certain distance metric between \mathbf{x} and \mathbf{x}' . The inner maximization problem is equivalent to constructing the strongest adversarial samples. And if l_∞ distance is employed as the distance metric $D(\mathbf{x}, \mathbf{x}')$, the inner maximization problem is equivalent to the adversarial problem solved by PGD, i.e., (4). The outer minimization is the standard training procedure to minimize the loss of a DNN. Recent work shows that this straightforward method is one of the most effective defenses against adversarial samples (Madry et al. 2017; Tramèr et al. 2017; Cai et al. 2018)

PGD Adversarial Training The fact that PGD adversary is a first-order universal adversary implies that robustness against PGD should yield robustness against all first-order adversaries (Madry et al. 2017). Hence, Madry et al. propose to adversarially train a robust classifier using PGD attack. Specifically, in each training iteration, PGD is applied to generate a minibatch of adversarial samples to update the current network. In the training process, a steady decrease of the training loss is observed, indicating the effectiveness of this training paradigm. Experiment results show that PGD adversarial trained models are robust against PGD attack as well as another strong attacks such as the CW_∞ attack (Carlini and Wagner 2017). We also experimentally found that their MNIST and CIFAR-10 models are indeed robust to a wide range of existing first-order attacks, including DeepFool (Moosavi-Dezfooli, Fawzi, and Frossard 2016), and Jacobian-based Saliency Map Attack (JSMA) (Papernot et al. 2016).

Ensemble Adversarial Training To scale up adversarial training to ImageNet-scale datasets, (Kurakin, Goodfellow, and Bengio 2016b) adversarially trains a model using a fast single-step attack method. However, their adversarially-trained model is vulnerable to multi-step white-box attacks (Kurakin, Goodfellow, and Bengio 2016b). Tramèr et al. further demonstrate that the model of Kurakin et al. is even vulnerable to black-box adversaries (Tramèr et al. 2017). To tackle this problem, Tramèr et al. propose a training methodology that incorporates adversarial samples transferred from other pre-trained models, called Ensemble Adversarial Training (EAT) (Tramèr et al. 2017). Intuitively, this approach increases the diversity of adversarial samples used for adversarial training. In their experiments, the models trained by EAT exhibit robustness against adversarial samples transferred from other holdout models, using various single-step and multi-step attacks.

3 Distributionally Adversarial Attack

This section describes our proposed DAA framework. We first interpret distributionally adversarial attack as WGFs, and then propose specific energy function to construct such a WGF, and finally propose particle-approximation methods to solve the DAA problem.

3.1 Adversarial Attack as WGFs

For a given DNN, the landscape of a loss function $\mathcal{L}(\mathbf{x}, y; \theta)$ constitutes a geometry structure indexed by input images. From a probability perspective, under regularized condition, it is natural to define a probability distribution for each input \mathbf{x} based on the loss-function landscape, i.e.,

$$p(\mathbf{x}, y; \theta) \propto \exp\{-\mathcal{L}(\mathbf{x}, y; \theta)\}.$$

Since y is deterministic given \mathbf{x} , we would omit y , and write $p(\mathbf{x}, y; \theta)$ as $p(\mathbf{x}; \theta)$ in the following for simplicity. Based on this, we explain our intuitions on generalizing adversarial attack on the space of probability measures in the following. First note that the objective of adversarial attack (4) is equivalently rewritten as:

$$\mathbf{x}' = \arg \max_{\mathbf{x}': D(\mathbf{x}, \mathbf{x}') < \alpha} \{\mathcal{L}(\mathbf{x}', y; \theta) - \mathcal{L}(\mathbf{x}, y; \theta)\}, \quad (8)$$

which describes the increase of loss with an adversarial sample. On the space of probability measure, the loss is instead describe by the energy functional $E(\mu)$, where it is reasonable to assume the minimum of $E(\mu)$ is obtained at $p(\mathbf{x}; \theta)$. Consequently, instead of finding an optimal adversarial sample \mathbf{x}' for each \mathbf{x} , DAA tries to find an optimal *adversarial distribution*, μ^* , such that μ^* is close to $p(\mathbf{x}; \theta)$ but increases $E(\cdot)$ maximally, i.e.,

$$\begin{aligned} \mu^* &= \arg \max_{\mu: W_2(\mu, p(\mathbf{x}; \theta)) < \alpha} \{E(\mu) - E(p)\} \\ &= \arg \max_{\mu: W_2(\mu, p(\mathbf{x}; \theta)) < \alpha} E(\mu). \end{aligned} \quad (9)$$

Theorem 3 *The solution μ^* of (9) is equivalently described by the following PDE:*

$$\partial_t \mu_t = -\nabla_{\mathbf{x}} \cdot \left(\mu_t \nabla_{\mathbf{x}} \left(\frac{\delta E}{\delta \mu_t}(\mu_t) \right) \right), \quad (10)$$

and $\mu^* = \mu_t$ where $t = \{\inf\{t' : \mu_0(\mathbf{x}) = p(\mathbf{x}; \theta), W_2(\mu_{t'}(\mathbf{x}), p(\mathbf{x}; \theta)) = \alpha\}\}$.

3.2 Energy Functional

It is crucial to define an energy functional as it directly affects adversarial-sample behaviors. Our guidance for designing an appropriate energy functional is that it should be simple enough to have a unique solution, *i.e.*, it should be convex w.r.t. μ on the space of probability measures. Different from standard WGF setting (Chen et al. 2018), which uses the KL divergence as the energy functional, we adopt the annealing idea in variational autoencoder (Yeung et al. 2017), and introduces an additional term from the loss to define a new energy functional as:

$$E(\mu) = \int_{\mu} \mathcal{L}(\mathbf{x}, y; \boldsymbol{\theta}) d\mu + c \cdot \text{KL}(\mu \| p), \quad (11)$$

where $\mathcal{L}(\mathbf{x}, y; \boldsymbol{\theta})$ is the loss of the system; $KL(\mu \| p)$ is the KL-divergence between the adversarial distribution μ and the optimal data distribution p ; and c is a hyperparameter balancing those two terms. Intuitively, (11) puts an emphasis on a good generalization error w.r.t. the adversarial distribution μ . Note the energy functional (11) is still convex w.r.t. μ , maintaining the optimality condition and making the solution much easier.

3.3 Optimization and Adversarial-Sample Generation

Note a close-formed solution of (10) is infeasible given the energy functional defined by (11). Following standard methods such as those in (Chen et al. 2018), we adopt particle approximation to solve (10). The idea is to approximate μ with a set of M particles $\{\mathbf{x}^{(i)}\}_{i=1}^M$, as

$$\mu \approx \frac{1}{M} \sum_{i=1}^M \delta_{\mathbf{x}^{(i)}}, \quad (12)$$

where $\delta_{\mathbf{x}}$ is a delta function with a spike at \mathbf{x} . Consequently, solving for the optimal μ corresponds to optimizing the particles as *adversarial samples* from the adversarial distribution. In the following, based on (Chen et al. 2018), we investigate two methods for particle approximation in the following: the Lagrangian blob method and the discrete-gradient-flow method.

Lagrangian Blob Method The idea is to use particle approximations directly in the original problem (10). Specifically, defined $\mathbf{v}_t \triangleq \nabla_{\mathbf{x}} \left(\frac{\delta E}{\delta \mu_t}(\mu_t) \right)$. According to (Carrillo, Craig, and Patacchini 2017), \mathbf{v}_t is interpreted as the velocity of a particle in the gradient flow. Consequently, Lagrangian blob methods evolve particles on a grid with a time-spacing h following the velocity \mathbf{v}_t (Carrillo, Craig, and Patacchini 2017), thus solving the WGF (10) is equivalent to evolving the particles along their velocities, *i.e.*, by solving

$$d\mathbf{x}^{(i)} / dt = \mathbf{v}_t(\mathbf{x}^{(i)}).$$

To calculate \mathbf{v}_t , we substitute the form of $E(\mu)$ in (11) into \mathbf{v}_t . First note that under the \mathcal{H} -Wasserstein distance metric

defined by (Liu et al. 2017), we have

$$\begin{aligned} \nabla_{\mathbf{x}} \left(\frac{\delta KL(\mu_t \| p)}{\delta \mu_t}(\mu_t) \right) &= \mathbb{E}_{\tilde{\mathbf{x}} \sim \mu_t} [\nabla_{\tilde{\mathbf{x}}} [p(\tilde{\mathbf{x}}) K(\mathbf{x}, \tilde{\mathbf{x}})] / p(\tilde{\mathbf{x}})] \\ &= \mathbb{E}_{\tilde{\mathbf{x}} \sim \mu_t} [K(\mathbf{x}, \tilde{\mathbf{x}}) \nabla_{\tilde{\mathbf{x}}} \log p(\tilde{\mathbf{x}}) + \nabla_{\tilde{\mathbf{x}}} K(\mathbf{x}, \tilde{\mathbf{x}})], \end{aligned} \quad (13)$$

where $K(\cdot, \cdot)$ is a kernel function such as the RBF kernel. For the first term in the right of (11), we have

$$\nabla_{\mathbf{x}} \left(\frac{\delta \int_{\mu} \mathcal{L}(\mathbf{x}, y; \boldsymbol{\theta}) d\mu}{\delta \mu_t}(\mu_t) \right) = \nabla_{\mathbf{x}} \mathcal{L}(\mathbf{x}, y; \boldsymbol{\theta}). \quad (14)$$

Combining Eq. 13 and 14, one ends up solving the following ordinary differential equation:

$$\begin{aligned} \frac{d\mathbf{x}}{dt} &= \nabla_{\mathbf{x}} \mathcal{L}(\mathbf{x}, y; \boldsymbol{\theta}) + \\ &\quad c \cdot \mathbb{E}_{\tilde{\mathbf{x}} \sim \mu_t} [K(\mathbf{x}, \tilde{\mathbf{x}}) \nabla_{\tilde{\mathbf{x}}} \log p(\tilde{\mathbf{x}}) + \nabla_{\tilde{\mathbf{x}}} K(\mathbf{x}, \tilde{\mathbf{x}})]. \end{aligned} \quad (15)$$

Considering a discrete approximation of μ_t as in (21), and further solving it with the Euler numerical method, (15) reduces to

$$\begin{aligned} \mathbf{x}_{\ell+1}^{(i)} &= \mathbf{x}_{\ell}^{(i)} + \nabla_{\mathbf{x}_{\ell}^{(i)}} \mathcal{L}(\mathbf{x}_{\ell}^{(i)}, y^{(i)}; \boldsymbol{\theta}) + \\ &\quad \frac{c}{M} \sum_{j=1}^M [K(\mathbf{x}_{\ell}^{(i)}, \mathbf{x}_{\ell}^{(j)}) \nabla_{\mathbf{x}_{\ell}^{(j)}} \log p(\mathbf{x}_{\ell}^{(j)}) + \nabla_{\mathbf{x}_{\ell}^{(j)}} K(\mathbf{x}_{\ell}^{(i)}, \mathbf{x}_{\ell}^{(j)})], \end{aligned} \quad (16)$$

where in contrast to the continuous case, we use ℓ to index the number of steps for the discretized particles.

Discrete Gradient Flows Another approximate solution for (10) is to use discrete gradient flows (DGFs). DGFs approximate (10) with a composition of a sequence of sub-optimization problems, called the Jordan-Kinderlehrer-Otto (JKO) scheme (Jordan, Kinderlehrer, and Otto 1998), *i.e.*, $\mu_t \approx \tilde{\mu}_L \circ \dots \circ \tilde{\mu}_1$, where $L = t/h$, and $\tilde{\mu}_{\ell}$ is the solution of the following functional optimization problem *:

$$\mu_n = \arg \max_{\mu \in P_2(R^r)} \{E(\mu) - \frac{1}{2h} W_2^2(\mu_{n-1}, \mu)\}. \quad (17)$$

We solve (17) by particle approximation, with gradient ascent on the particles. To this end, we need gradients for the two terms on the RHS of (17). Inspired by (Chen et al. 2018), we decompose the two terms and reorganize as:

$$\begin{aligned} E_1 &\triangleq \sum_{i=1}^M \left(\mathcal{L}(\mathbf{x}_{\ell}^{(i)}, y^{(i)}; \boldsymbol{\theta}) - c \log p(\mathbf{x}_{\ell}^{(i)}) \right) \\ E_2 &\triangleq \mathbb{E}_{\mu} [\log \mu] + \frac{1}{2h} W_2^2(\mu, p). \end{aligned}$$

The gradient of the first term can be easily calculated as

$$\begin{aligned} \frac{\partial E_1}{\partial \mathbf{x}_{\ell}^{(i)}} &= \nabla_{\mathbf{x}_{\ell}^{(i)}} \mathcal{L}(\mathbf{x}_{\ell}^{(i)}, y^{(i)}; \boldsymbol{\theta}) + c \nabla_{\mathbf{x}_{\ell}^{(i)}} \log p(\mathbf{x}_{\ell}^{(i)}) \\ &= (1 + c) \nabla_{\mathbf{x}_{\ell}^{(i)}} \mathcal{L}(\mathbf{x}_{\ell}^{(i)}, y^{(i)}; \boldsymbol{\theta}). \end{aligned} \quad (18)$$

*Note the difference between (17) and the original JKO scheme. (17) changes the original min to max because the flow direction is reversed.

For the E_2 term, we apply similar idea as (Chen et al. 2018) by introducing Lagrangian multipliers, resulting in

$$\frac{\partial E_2}{\partial \mathbf{x}_\ell^{(i)}} \approx c \cdot [\sum_j 2u_i v_j (\frac{d_{ij}}{\lambda} - 1) e^{-\frac{d_{ij}}{\lambda}} (\mathbf{x}^{(i)} - \mathbf{x}_{k-1}^{(j)})], \quad (19)$$

where λ , u_i and v_j are Lagrangian multipliers, and $d_{ij} = \|\mathbf{x}^{(i)} - \mathbf{x}_{k-1}^{(j)}\|_2^2$. For the sake of simplicity, we do not update u_i and v_j , but instead use a fixed scaling factor γ to approximate $u_i v_j$.

Adversarial-Sample Generation As mentioned, the particles $\{\mathbf{x}_\ell^{(i)}\}$ can be regarded as *adversarial samples* from the learned *adversarial distribution*. To get true adversarial samples with certain constraints, we propose two adversarial-sample generation methods based on the previously derived particle-optimization formula, named DAA-BLOB and DAA-DGF. DAA-BLOB substitutes the gradient used in PGD with the gradient derived in Eq. 16. Formally, in each iteration, \mathbf{x}^i is updated by

$$\mathbf{x}_{l+1}^{(i)} = \Pi_{\text{clip}}\{\mathbf{x}_l^{(i)} + \epsilon \cdot \text{sign}(\nabla_{\mathbf{x}_l^{(i)}} \mathcal{L}(\mathbf{x}_l^{(i)}, y^{(i)}; \theta)) + \quad (20)$$

$$\frac{c}{M} [\sum_{j=1}^M K(\mathbf{x}_l^{(i)}, \mathbf{x}_l^{(j)}) \nabla_{\mathbf{x}_l^{(j)}} \mathcal{L}(\mathbf{x}_l^{(j)}, y^{(j)}; \theta) + \nabla_{\mathbf{x}_l^{(j)}} K(\mathbf{x}_l^{(i)}, \mathbf{x}_l^{(j)})]\}.$$

DAA-DGF substitutes the gradient used in PGD with the combination of Eq. 18 and Eq. 19. Specifically, in each iteration, \mathbf{x}^i is updated by

$$\mathbf{x}_{l+1}^{(i)} = \Pi_{\text{clip}}\{\mathbf{x}_l^{(i)} + \epsilon \cdot \text{sign}(\nabla_{\mathbf{x}_l^{(i)}} \mathcal{L}(\mathbf{x}_l^{(i)}, y^{(i)}; \theta)) - \frac{2\gamma c}{1+c} \cdot [\sum_{j=1}^M (\frac{d_{ij}}{\lambda} - 1) e^{-\frac{d_{ij}}{\lambda}} (\mathbf{x}_l^{(i)} - \mathbf{x}_l^{(j)})]\}. \quad (21)$$

Optimization by Data Subsampling In theory, the adversarial distribution μ to be optimized corresponds to the data manifold. Thus a good discrete approximation to μ is to use all the testing samples. In practice, however, it is computationally infeasible to update the particles following (20) or (21), since the complexity is $\mathcal{O}(M^2)$ for each particle update. To mitigate this issue, we propose a subsampling method to update testing samples in an unbiased and computationally feasible way: First, testing samples are randomly permuted and divided into finite number of minibatches; then samples in each minibatch are updated sequentially for a certain number of steps. This procedure is iterated for multiple rounds. The full algorithm is shown in Algorithm 1.

Connection with PGD There are two situations in which the proposed DAA framework reduces to PGD. The first situation is when $c = 0$, where the second terms of both (20) and (21) become 0, making the two gradients degrade to the gradient used in PGD. The second case is when $M = 1$, meaning that DAA is equivalent to PGD when the data-manifold is approximated by only one sample. In this case, the second term of the gradient used in DAA-DGF will become 0, and the second term of the gradient used

Algorithm 1 DAA algorithm (untargeted attack)

Require: A classifier with loss function $\mathcal{L}(\mathbf{x}^i, y^i; \theta)$; testing dataset $\{\mathbf{x}^i, y^i\}_{i=1}^N$; minibatch size M ; step size ϵ ; predefined final perturbation size α ; total iterations L ; rounds R ; hyperparameter c or $\frac{2\gamma c}{1+c}$;

Random Start: $\mathbf{x}_0^i = \mathbf{x}^i + \gamma^i$ ($\gamma^i \sim \mathcal{U}(-\alpha, \alpha)$)

No Random Start: $\mathbf{x}_0^i = \mathbf{x}^i$

for $r = 0$ to $R - 1$ **do**

Randomly permute the testing samples

for $k = 0$ to $L/R - 1$ **do**

$l = rL/R + k$

for $j = 0$ to $N/M - 1$ **do**

Follow Eq. 20 or 21 to update the minibatch $\{\mathbf{x}_l^i, y_l^i\}$ ($i = jM + 1 \sim (j+1)M$), where

$\Pi_{\text{clip}}(\cdot) = \text{clip}_{[0,1]}(\text{clip}_{[\mathbf{x}^i - \alpha, \mathbf{x}^i + \alpha]}(\cdot))$ ($[0, 1]$ is the pixel value range, maybe $[-1, 1]$ or $[0, 255]$)

end for

end for

end for

in DAA-BLOB reduces to $c \cdot [K(\mathbf{x}_l^i, \mathbf{x}_l^i) \nabla_{\mathbf{x}_l^i} \mathcal{L}(\mathbf{x}_l^i, y^i; \theta) + \nabla_{\mathbf{x}_l^i} K(\mathbf{x}_l^i, \mathbf{x}_l^i)] = c \cdot \nabla_{\mathbf{x}_l^i} \mathcal{L}(\mathbf{x}_l^i, y^i; \theta)$. The relation indicates that PGD is a special case of the proposed DAA framework, which does not take generalization ability into account.

4 Experiment

We detail our experiments by comparing the proposed DAA with current state-of-the-art methods on four standard datasets in this section.

4.1 Setup

Datasets and Related Models The proposed DAA together with state-of-the-art methods, PGD and Momentum PGD, are evaluated and compared on four standard datasets, including MINST, Fashion MNIST (FMNIST), CIFAR10 and ImageNet. For MINST, the attack target is the state-of-the-art PGD-adversarially-trained MINST model provided by MadryLab (Madry et al. 2017). The defense architecture contains a convolutional neural network (CNN) with two convolutional layers and a fully connected layer. For FMNIST, we adversarially train a model by PGD as the target model. The network architecture consists of four convolutional layers and a fully connected layer with batch normalization. For CIFAR10, MadryLab’s PGD adversarially trained CIFAR10 model is adopted as the target model. The network architecture is a residual CNN consisting of five residual units and a fully connected layer. For ImageNet, we adopt the target model in (Kurakin, Goodfellow, and Bengio 2016c), which is an adversarially trained Inception ResNet-v2 model. It is worth noting that all above adversarially trained models used for evaluation are state-of-the-art defense models.

Implementation Details For all the methods related to kernel functions, an RBF kernel $K(\mathbf{x}, \mathbf{x}') =$

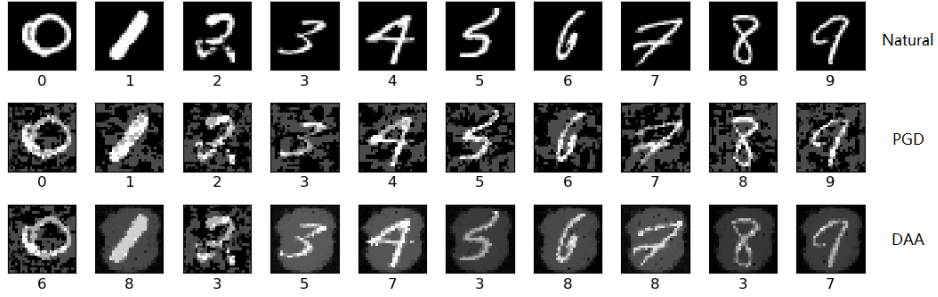


Figure 1: Comparison between PGD and DAA

Table 1: Empirical worst-case accuracy of Madry’s secret **MNIST** model under 200-step attacks with 50 random starts ($0.3/1.0 l_\infty$ perturbations). Loss 1: cross-entropy, Loss 2: CW_∞ loss

Rand+FGSM		PGD		Momentum PGD		DAA-BLOB		DAA-DGF	
Loss 1	Loss 2	Loss 1	Loss 2	Loss 1	Loss 2	Loss 1	Loss 2	Loss 1	Loss 2
93.48%	93.47%	89.49%	89.57%	89.29%	89.36%	88.79%	88.85%	88.92%	89.25%

Table 2: Parameters choice Loss 1: Cross-entropy, Loss 2: CW_∞ loss

	DAA-BLOB c		DAA-DGF $\frac{2\gamma c}{1+c}$	
	Loss 1	Loss 2	Loss 1	Loss 2
MNIST	1.0 ~ 2.0	10.0 ~ 20.0	0.001 ~ 0.01	0.01 ~ 0.1
FMNIST	1.0 ~ 2.0	10.0 ~ 20.0	0.001 ~ 0.01	0.01 ~ 0.1
CIFAR10	0.005 ~ 0.01	0.05 ~ 0.1	0.005 ~ 0.01	0.005 ~ 0.01
Imagenet	0.5	-	0.01	-

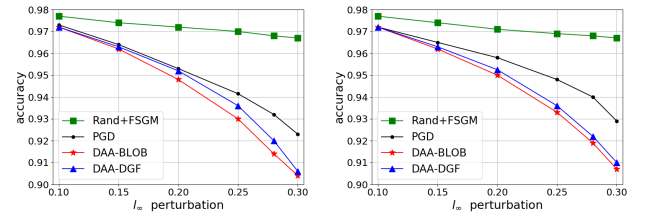
$\exp(-\|\mathbf{x} - \mathbf{x}'\|_2^2/h)$ is adopted. The bandwidth set as $h = med^2/\log M$, same as the kernel used in (Liu and Wang 2016) and (Chen et al. 2018). Here med is the median of the pairwise distance between particles. The minibatch size (number of particles) is set to 100 ~ 200 for computational feasibility. The specific parameter settings are listed in Table 2, where the discrepancy regarding the parameter choice on CIFAR10 is because the pixel values are in the range of $[0, 255]$. Full details can also be found in our code. All experiments are conducted on a single Titan V GPU under the white-box setting, where the adversary has full access to the target model including model weights.

4.2 Adversarial Perturbation Analysis

To intuitively understand the advantage of DAA over PGD, we plot ten natural samples and their PGD and DAA adversarial samples in Figure 1. For the ten samples, DAA is able to find their adversarial samples with a $0.3/1.0 l_\infty$ perturbation, whereas PGD with 50 random starts cannot. As shown in Figure 1, the perturbations generated by PGD tend to scatter throughout the images, whereas those of DAA are more focused around the target digits.

4.3 Empirical Results

MNIST We plot the averaged classification accuracy of MadryLab’s adversarially trained MNIST model under a single run of different attack algorithms in Figure 2. It is observed that the proposed DAA consistently outperforms other methods under different levels of l_∞ perturbations and



(a) Cross-entropy

(b) CW_∞ loss

Figure 2: Averaged classification accuracy of Madry’s adversarially trained MNIST model under a single run of different attacks

two different losses. To test its statistic significance, we also conduct t-tests between the accuracies reduced by PGD and DAA with random starts. T-test is used to assess how significant the differences are between two groups t-score is a ratio between the difference between two groups and the difference within the groups, and larger t-score indicates more difference between the two groups; p-value is the probability that the results from your sample data occurred by chance (Aankul). The t-score between the accuracies reduced by PGD and DAA-BLOB is 76.94 and the p-value is 0.0%. The t-score between the accuracies reduced by PGD and DAA-DGF is 75.95 and the p-value is also 0.0%. Those results suggest that both DAA-BLOB and DAA-DGF perform better than PGD in a statistical sense. In addition, we show the worst classification accuracy of Madry’s adversarially trained model under PGD, Momentum PGD and DAA with 50 random restarts in Table 1. It is seen that DAA-BLOB is able to reduce the classification accuracy to approximately 88.79% (with $c = 1.1$ and minibatch size of 200), outperforming the attacks listed in MadryLab’s white-box leaderboard.

Table 3: Empirical worst-case accuracy of adversarially trained **FMNIST** model under 100-step attacks with 10 random starts ($0.2/1.0$ l_∞ perturbations). Loss 1: cross-entropy, Loss 2: CW_∞ loss

Rand+FGSM		PGD		Momentum PGD		DAA-BLOB		DAA-DGF	
Loss 1	Loss 2	Loss 1	Loss 2	Loss 1	Loss 2	Loss 1	Loss 2	Loss 1	Loss 2
77.45%	77.21%	68.54%	68.94%	69.72%	69.51%	65.70%	66.64%	66.04%	66.60%

Table 4: Empirical worst-case accuracy of Madry’s adversarially trained **CIFAR10** model under a single run of 100-step attacks without random start ($8, 16/255$ l_∞ perturbations). Loss 1: cross-entropy, Loss 2: CW_∞ loss

l_∞	Rand+FGSM		PGD		Momentum PGD		DAA-BLOB		DAA-DGF	
	Loss 1	Loss 2	Loss 1	Loss 2	Loss 1	Loss 2	Loss 1	Loss 2	Loss 1	Loss 2
8/255	55.63%	55.05%	45.09%	46.27%	45.86%	46.76%	44.98%	46.30%	45.07%	46.31%
16/255	38.80%	37.78%	14.59%	16.06%	17.73%	18.70%	14.43%	16.05%	14.52%	16.06%

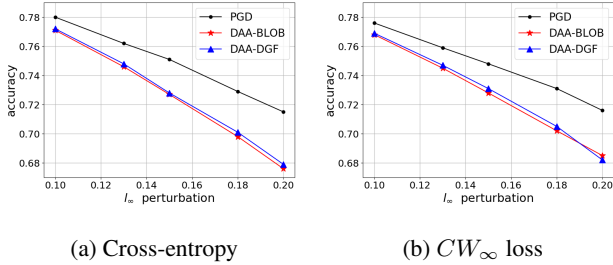


Figure 3: Averaged classification accuracy of adversarially trained FMNIST model under a single run of different attacks

FMNIST We next plot the classification accuracy of our adversarially trained FMNIST model under a single run of different attack algorithms in Figure 3. Similarly, the proposed DAA-based methods outperform the state-of-the-art PGD method. The two variants, DAA-BLOB and DAA-DGF, are comparable. The t-score between the accuracies reduced by PGD and DAA-BLOB with random starts is 119.24 and the p-value is 0.0%. The t-score between the accuracies reduced by PGD and DAA-DGF is 109.75 and the p-value is also 0.0%. The worst accuracy under white-box PGD, Momentum PGD and DAA with 10 random starts are listed in Table 3, suggesting the advance of the proposed DAA framework over PGD and Momentum PGD.

CIFAR10 The classification accuracy of Madry’s adversarially trained model under a single run of PGD, Momentum PGD and DAA without random start are shown in Table 4. As can be seen, the adversarially-trained model only achieves weak robustness, *i.e.*, a 100-step PGD with $16/255$ l_∞ perturbations reduces the accuracy to 14.59%, while DAA only reduces it to 14.43%. We conjecture this is because the data are too complex and sparse, making the particle approximation with testing samples in DAA badly represent the true data manifold. As a result, the learned adversarial samples are similar to those generated by PGD. This argument is also validated by (Recht et al. 2018), which shows that existing high-accuracy CIFAR10 classifiers does not generalize well to a truly unseen CIFAR10 testing set.

Table 5: Empirical worst-case accuracy of adversarially trained Inception ResNet v2 under FGSM and 50-step DAA attacks ($2/255$ l_∞ perturbations). Acc 1: Top 1 accuracy, Acc 2: Top 5 accuracy

Rand+FGSM		DAA-BLOB		DAA-DGF	
Acc 1	Acc 2	Acc 1	Acc 2	Acc 1	Acc 2
69.98%	91.08%	16.53%	35.40%	16.43%	35.32%

ImageNet In Table 5, we show the worst classification accuracies of the ensemble adversarial trained Inception ResNet-v2 under 50-step targeted Rand+FGSM and DAA attacks, using the least likely class as the target. It is shown that Rand+FGSM with $2/255$ l_∞ perturbations (approximately $0.0157/2.0$ l_∞ perturbations after normalization) can reduce the accuracy of the Inception model to approximately 70% (Kurakin, Goodfellow, and Bengio 2016b), while 50-step DAA can dramatically reduce it to 16.43%. This indicates the ensemble adversarial trained imagenet model is still vulnerable to well-designed iterative attacks.

5 Discussion

Madry et al. show that PGD is a universal first-order l_∞ attack, thus there is not existing first-order attack algorithms that outperform PGD under a white-box setting. Even for MI-FGSM, which won the NIP2017 competition under a black-box setting, we found that even its PGD variant with several step updates cannot outperform standard PGD under a white-box setting, let alone MI-FGSM. In this paper, we generalize PGD on the space of data distributions. Our theoretical derivations and experiments validate the effectiveness of our framework. To the best of our knowledge, the proposed DAA framework is the only first-order l_∞ attack algorithm that can really outperform PGD, especially on robust adversarially trained models. To further attack those adversarially trained models with small l_∞ perturbations, we might need to involve higher-order information, which is usually very computationally expensive. In practice, those l_∞ adversarially trained models can also be further attacked by perturbing few pixels with large l_∞ perturbations, which still yields small l_1 or l_2 distance (Chen et al. 2017). However, such a change sometimes even leads to misclassification by human. Moreover, it is unfair to compare an l_1 or l_2

attack with an l_∞ attack (PGD) on l_∞ adversarially trained models.

6 Conclusion

We generalize PGD on the space of data distributions, by learning an adversarial distribution that maximally increases the generalization risk of a model. To solve the adversarial-distribution problem, we define a new energy functional to better reflex the data manifold in the WGF framework. When adopting particle approximation, non-targeted/targeted adversarial samples can be generated by solving the corresponding WGF problem, which is closely related to standard PGD method. An extensive evaluation shows that our distributionally adversarial attack outperforms PGD and Momentum PGD, achieving state-of-the-art attack results on the adversarially trained defense models that demonstrated notable robustness against first-order l_∞ attacks.

References

- [Aankul] Aankul, A. T-test using python and numpy.
- [Ambrosio, Gigli, and Savaré 2008] Ambrosio, L.; Gigli, N.; and Savaré, G. 2008. *Gradient flows: in metric spaces and in the space of probability measures*. Springer Science & Business Media.
- [Athalye, Carlini, and Wagner 2018] Athalye, A.; Carlini, N.; and Wagner, D. 2018. Obfuscated gradients give a false sense of security: Circumventing defenses to adversarial examples. *arXiv preprint arXiv:1802.00420*.
- [Cai et al. 2018] Cai, Q.-Z.; Du, M.; Liu, C.; and Song, D. 2018. Curriculum adversarial training. *arXiv preprint arXiv:1805.04807*.
- [Carlini and Wagner 2017] Carlini, N., and Wagner, D. 2017. Towards evaluating the robustness of neural networks. In *Security and Privacy (SP), 2017 IEEE Symposium on*, 39–57. IEEE.
- [Carlini et al. 2017] Carlini, N.; Katz, G.; Barrett, C.; and Dill, D. L. 2017. Ground-truth adversarial examples. *CoRR abs/1709.10207*.
- [Carrillo, Craig, and Patacchini 2017] Carrillo, J. A.; Craig, K.; and Patacchini, F. S. 2017. A blob method for diffusion. *arXiv preprint arXiv:1709.09195*.
- [Chen et al. 2017] Chen, P.-Y.; Sharma, Y.; Zhang, H.; Yi, J.; and Hsieh, C.-J. 2017. Ead: elastic-net attacks to deep neural networks via adversarial examples. *arXiv preprint arXiv:1709.04114*.
- [Chen et al. 2018] Chen, C.; Zhang, R.; Wang, W.; Li, B.; and Chen, L. 2018. A unified particle-optimization framework for scalable bayesian sampling. *arXiv preprint arXiv:1805.11659*.
- [Cho et al. 2014] Cho, K.; Van Merriënboer, B.; Gulcehre, C.; Bahdanau, D.; Bougares, F.; Schwenk, H.; and Bengio, Y. 2014. Learning phrase representations using rnn encoder-decoder for statistical machine translation. *arXiv preprint arXiv:1406.1078*.
- [Dong et al. 2018] Dong, Y.; Liao, F.; Pang, T.; Su, H.; Zhu, J.; Hu, X.; and Li, J. 2018. Boosting adversarial attacks with momentum. *arXiv preprint*.
- [Goodfellow, Shlens, and Szegedy 2014] Goodfellow, I. J.; Shlens, J.; and Szegedy, C. 2014. Explaining and harnessing adversarial examples. *arXiv preprint arXiv:1412.6572*.
- [Jordan, Kinderlehrer, and Otto 1998] Jordan, R.; Kinderlehrer, D.; and Otto, F. 1998. The variational formulation of the fokker–planck equation. *SIAM journal on mathematical analysis* 29(1):1–17.
- [Krizhevsky, Sutskever, and Hinton 2012] Krizhevsky, A.; Sutskever, I.; and Hinton, G. E. 2012. Imagenet classification with deep convolutional neural networks. In *Advances in neural information processing systems*, 1097–1105.
- [Kurakin, Goodfellow, and Bengio 2016a] Kurakin, A.; Goodfellow, I.; and Bengio, S. 2016a. Adversarial examples in the physical world. *arXiv preprint arXiv:1607.02533*.
- [Kurakin, Goodfellow, and Bengio 2016b] Kurakin, A.; Goodfellow, I.; and Bengio, S. 2016b. Adversarial machine learning at scale. *arXiv preprint arXiv:1611.01236*.
- [Kurakin, Goodfellow, and Bengio 2016c] Kurakin, A.; Goodfellow, I. J.; and Bengio, S. 2016c. Adversarial machine learning at scale. *CoRR abs/1611.01236*.
- [Liu and Wang 2016] Liu, Q., and Wang, D. 2016. Stein variational gradient descent: A general purpose bayesian inference algorithm. 2378–2386.
- [Liu et al. 2017] Liu, Y.; Ramachandran, P.; Liu, Q.; and Peng, J. 2017. Stein variational policy gradient. *CoRR abs/1704.02399*.
- [Madry et al. 2017] Madry, A.; Makelov, A.; Schmidt, L.; Tsipras, D.; and Vladu, A. 2017. Towards deep learning models resistant to adversarial attacks. *arXiv preprint arXiv:1706.06083*.
- [Moosavi-Dezfooli, Fawzi, and Frossard 2016] Moosavi-Dezfooli, S.-M.; Fawzi, A.; and Frossard, P. 2016. Deepfool: a simple and accurate method to fool deep neural networks. In *Proceedings of the IEEE Conference on Computer Vision and Pattern Recognition*, 2574–2582.
- [Papernot et al. 2016] Papernot, N.; McDaniel, P.; Jha, S.; Fredrikson, M.; Celik, Z. B.; and Swami, A. 2016. The limitations of deep learning in adversarial settings. In *Security and Privacy (EuroS&P), 2016 IEEE European Symposium on*, 372–387. IEEE.
- [Recht et al. 2018] Recht, B.; Roelofs, R.; Schmidt, L.; and Shankar, V. 2018. Do cifar-10 classifiers generalize to cifar-10? *arXiv preprint arXiv:1806.00451*.
- [Silver et al. 2016] Silver, D.; Huang, A.; Maddison, C. J.; Guez, A.; Sifre, L.; Van Den Driessche, G.; Schrittwieser, J.; Antonoglou, I.; Panneershelvam, V.; Lanctot, M.; et al. 2016. Mastering the game of go with deep neural networks and tree search. *nature* 529(7587):484–489.
- [Szegedy et al. 2013] Szegedy, C.; Zaremba, W.; Sutskever, I.; Bruna, J.; Erhan, D.; Goodfellow, I.; and Fergus, R. 2013. Intriguing properties of neural networks. *arXiv preprint arXiv:1312.6199*.

- [Tramèr et al. 2017] Tramèr, F.; Kurakin, A.; Papernot, N.; Goodfellow, I.; Boneh, D.; and McDaniel, P. 2017. Ensemble adversarial training: Attacks and defenses. *arXiv preprint arXiv:1705.07204*.
- [Yeung et al. 2017] Yeung, S.; Kannan, A.; Dauphin, Y.; and Fei-Fei, L. 2017. Tackling over-pruning in variational autoencoders. In *ICML Workshop on Principled Approaches to Deep Learning*.